Research Article Vol. 2, No. 9 / September 2015 / Optica 797

Midinfrared supercontinuum generation from 2 to 6 μm in a silicon nanowire

Neetesh Singh,[1,*] Darren D. Hudson,[1] Yi Yu,[2] Christian Grillet,[3] Stuart D. Jackson,[4] Alvaro Casas-Bedoya,[1] Andrew Read,[5] Petar Atanackovic,[5] Steven G. Duvall,[5] Stefano Palomba,[1] Barry Luther-Davies,[2] Stephen Madden,[2] David J. Moss,[6] and Benjamin J. Eggleton[1]

[1]Center for Ultrahigh Bandwidth Devices for Optical Systems (CUDOS), Institute of Photonics and Optical Science (IPOS), School of Physics, University of Sydney, NSW 2006, Australia
[2]CUDOS, Laser Physics Center, Research School of Physics and Engineering, Australian National University, Canberra, ACT 0200, Australia
[3]Université de Lyon, Institut des Nanotechnologies de Lyon INL-UMR5270, CNRS, Ecole Centrale de Lyon, Ecully, F-69134, France
[4]Faculty of Science and Engineering, Macquarie University, NSW 2109, Australia
[5]Silanna Semiconductor, 8 Herb Elliot Ave., Sydney Olympic Park, NSW 2127, Australia
[6]School of Electrical and Computer Engineering, RMIT University, Melbourne, Victoria 3001, Australia
*Corresponding author: neetesh@physics.usyd.edu.au

Received 13 July 2015; revised 12 August 2015; accepted 13 August 2015 (Doc. ID 245639); published 4 September 2015

Silicon has attracted great interest as a platform for both linear and nonlinear integrated photonics for over 15 years. While its primary applications have been in the telecom window (near 1.5 μm), the capability of exploiting its full transparency window to 8 μm in the mid-IR is highly attractive, since this will open it up to entirely new applications in fields such as spectroscopy, chemical and biological sensing, and free-space communications. However, while silicon-on-insulator has shown great promise just beyond the telecommunications window [to the shortwave IR band (2.5 μm)], its wavelength range has been limited to < 4 μm by absorption in the silica cladding layer. Here, we demonstrate octave-spanning supercontinuum generation in silicon, covering a continuous spectral range from 1.9 to beyond 6 μm in dispersion-engineered silicon-on-sapphire (SOS) nanowires. This represents both the widest spectrum and longest wavelength generated to date in any silicon platform, and establishes SOS as a promising new platform for integrated nonlinear photonics in the mid-IR.

OCIS codes: (130.5990) Semiconductors; (190.4390) Nonlinear optics, integrated optics; (230.6080) Sources; (320.7110) Ultrafast nonlinear optics.

http://dx.doi.org/10.1364/OPTICA.2.000797

1. INTRODUCTION

The midinfrared (mid-IR) is an important spectral range for a wide range of applications in medicine, security, food production, and telecommunications that impact almost all aspects of our society. One application that has received a lot of interest is on-chip sensing of molecules using a broadband source in the mid-IR (>2.5 μm). In this range, molecules that are important for health, security screening, and environmental sensing have fundamental rotational–vibrational absorption lines. Probing with mid-IR light allows them to be detected with high sensitivity (at levels of parts per billion or even trillion) due to the strong photon–molecule interaction. Sensing devices in integrated form would offer the greatest benefits in cost, footprint, and performance, and this has motivated the search for efficient platforms for integrated photonics in the mid-IR.

Both silicon and chalcogenide glass have shown great promise as platforms for the mid-IR, since their transparency in the mid-IR extends to more than 8 μm for silicon and beyond 10 μm for chalcogenide glasses. Chalcogenide glass has demonstrated many linear and even nonlinear optical functions including broadband supercontinuum generation (SCG) out to 13 μm [1,2]. On the other hand, silicon offers significant advantages over many other materials for its compatibility with electronic integrated circuit manufacturing (CMOS) as well as extremely high material stability and reliability. Its successes include signal processing [3], optical interconnects [4,5], fundamental optical physics [6], and quantum optical applications such as photon pair sources [7,8], as well as uses in the shortwave IR (SWIR) band near 2.5 μm, where the well-known problem of two-photon absorption (TPA) prevents very high parametric gain [9,10].

However, silicon—in its common embodiment of silicon-on-insulator (SOI)—has struggled to operate much beyond the SWIR band (centered at 2.5 μm), despite some promising reports of nonlinear optics out to 3.5 μm [11–14], due primarily to absorption of the silica cladding layers. Among the new platforms proposed for the mid-IR [15,16], silicon-on-sapphire (SOS) has attracted significant interest [17–22] because of the transparency of the sapphire substrate to beyond 5 μm, and high-quality optical

waveguides have been reported out to this wavelength. SOS was, in fact, the first SOI technology to be developed and has been used commercially for over 50 years for electronics; the excellent insulator properties of sapphire yield low parasitic capacitance, which makes SOS the platform of choice for high-speed electronics, and in particular rf electronics [23].

The first SOS-based waveguides reported in 2010 had propagation losses of 4.3 dB/cm at 4.5 μm [17]. This work was soon followed by the demonstration of various devices including ring resonators [18–20], grating couplers, and slot waveguides [21,22].

However, the nonlinear optical performance of SOS—critical for many functions such as broadband spectrum generation—has remained unproven. Indeed, the recent discovery [24–26] that significant multiphoton absorption (three- and four-photon) exists in silicon even beyond 2.5 μm, where TPA vanishes, has raised some doubts about silicon as a viable nonlinear optical platform for the mid-IR.

Here, we report the first continuous octave-spanning supercontinuum, as well as the longest wavelength produced to date in the mid-IR, in a silicon platform. We achieve this by exploiting low-loss dispersion-engineered SOS nanowires. These results not only firmly establish silicon, and SOS in particular, as a viable platform for integrated nonlinear photonics in the mid-IR but also achieve the critical milestone of continuous octave-spanning SCG directly in silicon.

This result is a clear demonstration that the observed high-order multiphoton absorption in silicon in the mid-IR does not pose an insurmountable barrier to exploiting nonlinear effects in this wavelength range. Furthermore, we show theoretically that silicon is capable of generating light as far out as 8 μm [27].

2. EXPERIMENTS AND RESULTS

We designed and fabricated SOS nanowires in order to achieve optimal dispersion (low and anomalous) at the pump wavelength in the region where multiphoton absorption and linear propagation losses are low. The dispersion and effective index profile along with the fundamental mode for a 2.4 μm by 0.48 μm nanowire is shown in Fig. 1. Although the nanowire supports a second mode, its group velocity dispersion is quite different from that of the fundamental mode, so intermodal coupling has a negligible effect on the soliton fission process [28].

To minimize propagation loss, the nanowires were treated with chemical oxidation and oxide stripping to reduce surface roughness (see Supplement 1) [29–31]. This reduced the losses to 1 ± 0.3 dB/cm at 4 μm. The use of a relatively wide nanowire, to obtain appropriate dispersion for soliton-based SCG, also had the benefit of improving the mode confinement, thereby reducing the contribution from the surface roughness to the loss. The measured loss spectrum is shown in Fig. 2, where the peak between 3.3 and 3.4 μm represents C-H absorption due to contaminants on the nanowire surface. We note that tapered or grating couplers were not employed to reduce end-fire coupling loss, and therefore we incurred 9 dB/facet loss, with 20 dB total insertion loss. [18].

The SCG experiments, shown in Fig. 1, were performed by coupling the output of a tunable optical parametric amplifier [2], producing 320 fs wide pulses at 3.7 μm at a repetition rate (R_p) of 20 MHz, into the TE mode of the nanowire. The output was collimated and passed through a monochromator (see Supplement 1) and detected with two mid-IR detectors with

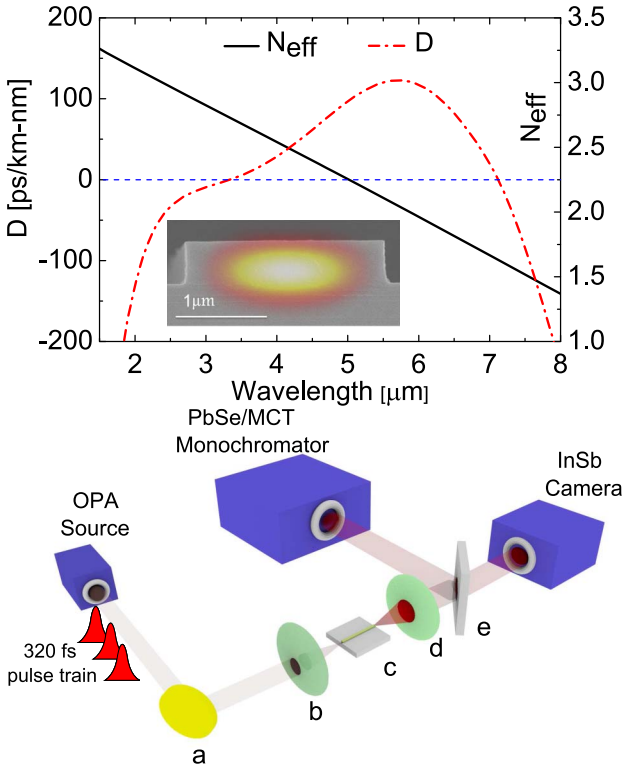

Fig. 1. Top: Calculated dispersion (D) and effective index (N_{eff}) curve for the SOS nanowire with a cross section of 2400 nm by 480 nm shown in inset, having zero dispersion wavelengths at 3.3 and 7.1 μm (see Methods section). Bottom: Experimental setup. a, gold mirror; b, Geltech BD2 chalcogenide lens, NA (= 0.85); c, chip; d, reflective microscope objective, NA (= 0.5); e, beam splitter, which was replaced by gold mirror during measurements.

different operating ranges (PbSe at 1.5–4.8 μm and MCT at 4–6.5 μm).

Figure 3(a) shows the experimentally observed output spectra for different coupled input peak powers, from 200 W to 2.5 kW, as well as the results of simulations [Fig. 3(b)]. The widest continuous spectrum at the −30 dB signal level is 1.53 octaves,

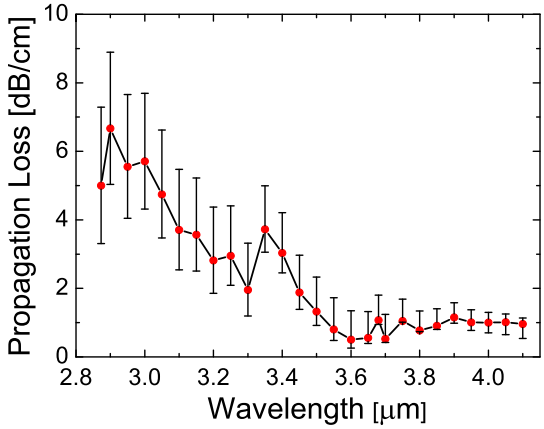

Fig. 2. SOS propagation loss obtained with a low-power tunable OPA source to avoid any nonlinear effects. The peak between 3.3 and 3.4 μm represents C-H absorption. Error bars include uncertainty in streak analysis, coupling coefficient, and detectivity of the detector.

Table 1. Supercontinuum Results

Coupled Power (kW)	Spectral Output Range (μm), at −30 dB	Octaves
2.5	2–5.56	1.47
1.82	1.9–5.5	1.53
1.06	2–5.12	1.31
0.52	2.12–4.62	1.12
0.2	2.86–4.2	0.55

achieved with 1.82 kW input power, as shown in Table 1. Furthermore, at −45 dB, which is still well above the noise floor, light is generated beyond 6 μm. (Note that the slight offset of the noise floor at the short and long wavelength edges was due to dissimilar noise levels of the two detectors, arising from their different active areas.) We also measured the nonlinear transmission, shown in Fig. 4, since this is expected to be appreciable at such high peak intensities in this wavelength range [24]. The observed trend is similar to that reported for SOI waveguides [24], with the onset of nonlinear loss occurring near 1 GW/cm^2 and strong saturation of the transmission occurring near 10 GW/cm^2. The maximum fluence reached was just over 0.04 J/cm^2—well under the damage threshold of silicon, and thus no input facet damage was observed, unlike in SOI [24,32,33]. The experimental results are in reasonable agreement with modeling using the absorption

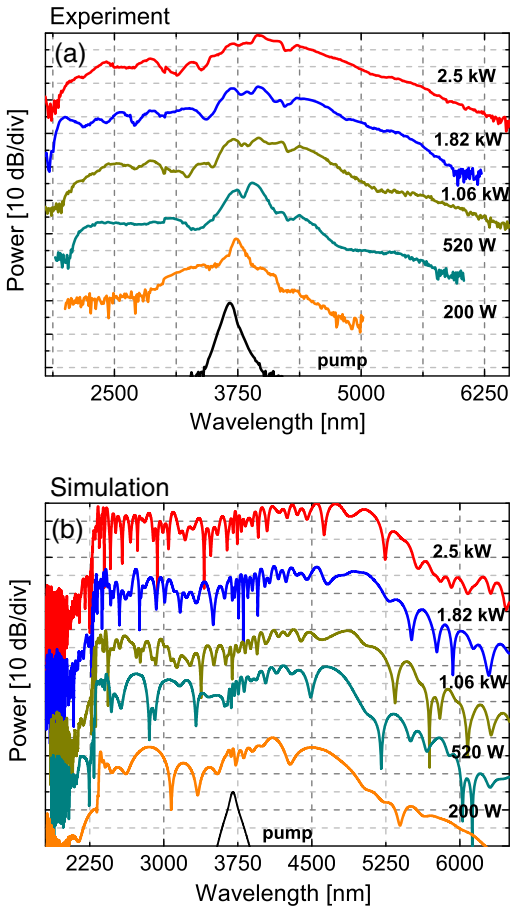

Fig. 3. (a) Experimental data with input peak power ranging from 200 W to 2.5 kW and (b) simulation results. Here, the pump corresponds to 7 W.

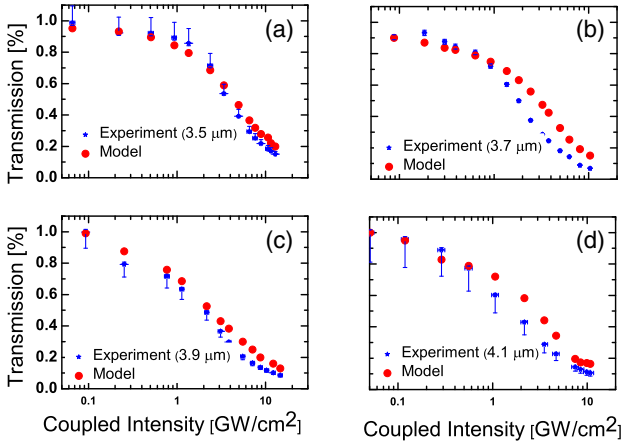

Fig. 4. Transmission versus coupled intensity at the input of a 5 μm by 0.5 μm SOS waveguide. (a)–(d) Experimental and calculated transmission at (a) 3.5 μm, (b) 3.7 μm, (c) 3.9 μm, and (d) 4.1 μm. Error bars include uncertainty in coupling coefficient, detectivity, calibration, and nonlinear power response error of the detector.

coefficients from [24], suggesting that four-photon absorption (4PA) is the main cause of the nonlinear reduction in transmission. The slight discrepancy could be accounted for by the uncertainty in free carrier absorption due to variation in the free carrier lifetime from nanowire surface effects and defects at the silicon–sapphire interface.

3. NUMERICAL MODELING AND DISCUSSION

To model the SCG, we use the nonlinear Schrödinger equation:

$$\frac{\partial E}{\partial z} = -\frac{\alpha(\omega)}{2}E + \sum_{m\geq 2}\frac{i^{m+1}\beta_m}{m!}\frac{\partial^m E}{\partial t^m} + i\left(\gamma(\omega_0) + i\gamma'\frac{\partial}{\partial t}\right)E \times \int_{-\infty}^{t} R(t-t')|E|^2 \mathrm{d}t' - \left(\frac{\gamma_{4pa}}{2A_{\mathrm{eff}}^3}|E|^6 - 3pa(\omega)|E|^4 - \frac{\sigma}{2}(1+i\mu)N_c\right)E.$$

Here, E is the electric field envelope, $\alpha(\omega)$ is the linear propagation loss, $A_{\mathrm{eff}} = |\int(E\times H^*)\cdot\hat{z}\mathrm{d}A|^2/\int|(E\times H^*)\cdot\hat{z}|^2\mathrm{d}A$ [34] is the effective mode area at the pump wavelength, β_m is the mth dispersion order, and $R(t)$ includes instantaneous electronic and delayed Raman responses (negligible in silicon); $\sigma(= 8.26\times10^{-21}$ m$^2)$, $\mu(= 3.16)$, and N_c, where $\frac{\partial N_c}{\partial t} = \frac{\gamma_{4pa}|E|^8}{4\hbar\omega A_{\mathrm{eff}}^4} - \frac{N_c}{\tau}$, are free carrier parameters, and γ_{4pa} is the 4PA coefficient [24,25]. For such a broad supercontinuum, the frequency dependence of the nonlinearity parameter $\gamma(\omega)$ is accounted for by $\frac{\gamma'(\omega_0)}{\gamma(\omega_0)} = \frac{1}{\omega_0} + \frac{1}{n_2}\frac{\partial n_2}{\partial\omega} - \frac{1}{A_{\mathrm{eff}}}\frac{\partial A_{\mathrm{eff}}}{\partial\omega}$, where $\frac{\partial n_2}{\partial\omega}$ is negligible for silicon in the operating wavelength range and the last term is -2×10^{-15} s [35].

Since the signal generation is prominent in the region where three-photon absorption is dominant (2.2–3.2 μm), we included its frequency dependence, denoted by $3pa(\omega)$. Here, $3pa(\omega) = 3pa(\omega_0) + i3pa'\frac{\partial}{\partial t}$, where $3pa(\omega_0)$ is zero and $3pa' = \frac{1}{2A_{\mathrm{eff}}^2}\left(\frac{\partial\gamma_{3pa}}{\partial\omega} - \frac{\gamma_{3pa}}{A_{\mathrm{eff}}}\frac{\partial A_{\mathrm{eff}}}{\partial\omega}\right)$, where the last term is zero as γ_{3pa} at ω_0 is negligible, and $\frac{\partial\gamma_{3pa}}{\partial\omega}$ is 7×10^{-42} m^3 sW^{-2}.

We neglected any nonlinear contribution from sapphire, because only 13% of the total power of the pump wave was propagating in the substrate and sapphire's Kerr index (n_2) is much smaller than silicon [36]. The higher linear losses on the short wavelength side in Fig. 2 are accounted for by the frequency-dependent loss parameter, $\alpha(\omega) = \alpha(\omega_0) + \partial\alpha/\partial\omega(\omega - \omega_0)$, causing less than 2 dB signal reduction due to the continuous feedback from the pump into the dispersive wave following soliton fission [shown in Fig. 5(b)]. We used 320 fs pulses with peak power levels consistent with the experiment, with waveguide parameter $\alpha(\omega_0) = 1$ dB/cm, $A_{\text{eff}} = 1.15\ \mu\text{m}^2$, and $n_2 = 6 \times 10^{-5}\ \text{cm}^2/\text{GW}$ [24].

The spectral broadening shown in Fig. 3 is chiefly governed by higher-order soliton propagation, which broadens the spectrum around the pump wavelength via the soliton fission process [35], while at the same time generating phase-matched dispersive waves in the normal dispersion region below 3.3 μm [37,38]. The dispersive waves were phase matched with the soliton waves generated with 3.7 μm pump, satisfying $\sum_{m=2}^{\infty} \frac{\beta_m(\omega_s)}{m!}\Omega_d^m = \frac{1}{2}\gamma P_s$, where $\Omega_d = \omega_d - \omega_s$, ω_s and ω_d [39] are frequencies of soliton and dispersive waves, respectively, and P_s is the peak power of soliton after fission. The calculated soliton fission length is 8 mm, in agreement with Fig. 5, and the soliton number is 143 at a peak power of 2.5 kW.

In order to investigate the dependence of the nanowire's nonlinear response to pump wavelength over the range where the SOS displays the combination of low linear propagation loss, lower nonlinear transmission loss, and smaller mode area, the optical parametric amplifier (OPA) was scanned from 3.5 to 4 μm. Only a 5% improvement in γ was gained by tuning the pump from 3.7 μm to over 3.5 μm.

The SCG was mainly limited by 4PA, causing high loss as well as narrowing of the spectrum, while free carrier effects were not as significant, since $R_p\tau < 0.06$ and the generated carriers lagged behind the pulse (unlike picosecond pulses). We note that the gradual decline in signal at the long wavelength side (5–6 μm) is expected regardless of nonlinear absorption (as confirmed by turning off the 4PA component in the modeling [35]) or attenuation due to the intrinsic multiphoton edge of sapphire in the mid-IR [15,40]. With further improvement in the design, it would be possible to exploit the long wavelength dispersive wave, as we demonstrate below. In addition, the calculated degree of first-order spectral coherence $|g_{12}^{(1)}| > 0.5$ was obtained from 3.6 to 4.7 μm, which can be improved with shorter input pulses and waveguide [41].

The residual discrepancy between theory and experiment below 2.25 μm can be attributed to fabrication uncertainty in the nanowire dimensions. This has a strong effect on the dispersion profile, which in turn can substantially change the soliton dynamics that affect phase matching for the dispersive waves. Including other effects such as input pulse chirp and the frequency dependence of both n_2 and A_{eff} in the model did not produce any significant spectral shift and can be ruled out as a possible source of the discrepancy. The mismatch in signal drop <3.2 μm could be due to uncertainty in high propagation losses at shorter wavelengths (Fig. 2), water, and C-H absorption. At low power, however, uncertainty in the coupled peak power may be responsible for the discrepancy.

To determine the sensitivity of the dispersion parameters to variations in the nanowire dimensions, we calculated them [β_2, β_3, and zero dispersion wavelength (ZDW) for the first zero of β_2] for various heights and widths for TE polarization. Figure 6 shows the results, where we observed a large shift of 0.8 μm in the ZDW for a change in height of only 20 nm, which was the difference between the measured height of our nanowire and the designed 500 nm. Moreover, the analysis illustrates a slightly nonlinear dependence of the ZDW on nanowire width, suggesting that a tighter tolerance is expected for any variation in height. For example, a single-mode nanowire operating at a pump wavelength of 3.7 μm would experience a shift of 400 nm in ZDW from just a 2% change in height compared to a 25% change in the width. This is because the aspect ratio of mid-IR nanowires tends to be higher than those designed for the near-IR [42]. Hence, slight variations in height can change the mode confinement significantly. As a result, a high precision in fabrication is required, particularly in height, for nonlinear processes such as SCG in high index contrast mid-IR waveguides.

In this work the supercontinuum-generated spectrum covered over 60% of silicon's transparency window. To access

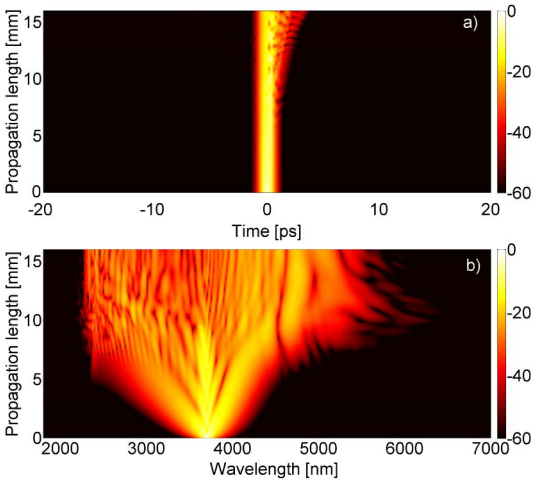

Fig. 5. Simulated (a) temporal evolution and (b) spectral evolution along the waveguide at a peak power of 2.5 kW.

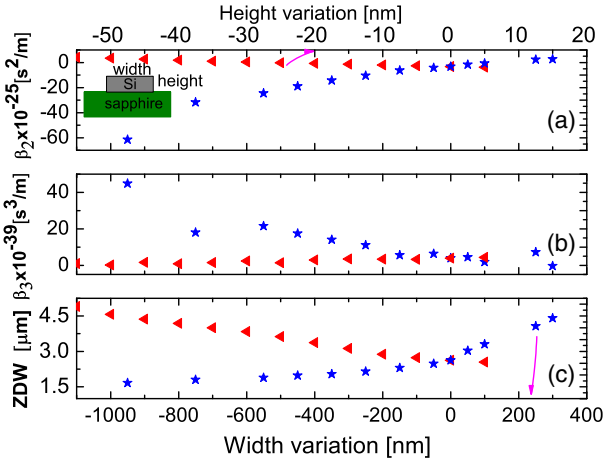

Fig. 6. Calculation of the dependence of SOS dispersion on nanowire dimension. Here, the width is varied from 2.4 μm for a constant height of 500 nm, while the height is varied from 500 nm for a constant width of 2.4 μm. (a) β_2, (b) β_3 (at 3.7 μm), and (c) ZDW dependence on width and height variations.

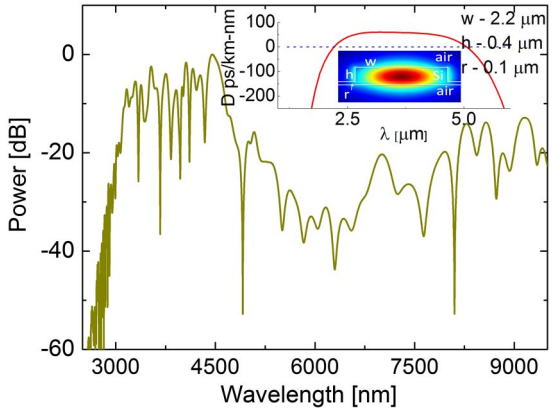

Fig. 7. Simulated spectral broadening of silicon rib nanowire (inset) with pumping at 4 μm generating a dispersive wave beyond the second ZDW at 5 μm.

the remaining long wavelength region, one would need to exploit dispersive waves, just as in the short wavelength side (below 3.5 μm) in Fig. 3. In Fig. 7 we show one of the possible structures of a suspended silicon rib nanowire designed to avoid any substrate-related multiphonon losses, which has flat dispersion over a 1 μm range with the second ZDW around 5 μm.

We modeled SCG in a 1.6 cm long suspended nanowire with a coupled peak power of 1 kW at 4 μm (to minimize multiphoton absorption) with a 320 fs pulse. To include the linear propagation loss for a suspended structure, we used a conservative estimate of 4 dB/cm based on [43]. The generated spectrum, with a dispersive wave beyond 6 μm, is shown in Fig. 7. Nevertheless, no signal was observed for wavelengths shorter than the first ZDW. This could be due to the extreme sensitivity of phase matching for the dispersive waves on the nanowire dimensions (shown in Fig. 6).

Although suspended structures avoid substrate-related absorption, they tend to be fragile. Thus an SOS based pillar waveguide can be employed to confine modes away from the substrate while achieving a flat dispersion across a wide bandwidth [44]. Additionally, further improvement in epitaxial growth methods would minimize the near-IR linear losses (by reducing lattice mismatch effects (e.g., dislocations) at the silicon and sapphire interface [45]). This should enable SCG coverage over the full transparency of silicon with a single nanowire.

4. CONCLUSION

In conclusion, we demonstrate continuous octave-spanning SCG in a silicon nanowire, covering the mid-IR wavelength range of 2–6 μm. This was achieved by pumping the dispersion-engineered SOS nanowire in the low linear and nonlinear loss mid-IR region. Theoretical calculations show that, in principle, spectral generation via SCG to beyond 8 μm is possible in silicon. This work opens the door for many new applications for CMOS-compatible silicon-based on-chip photonic signal processing, sensing, and broadband spectral emission in the mid-IR for a wide range of applications.

Funding. ARC, Laureate Fellowship (FL120100029); CUDOS (CE110001018); Discovery Early Career Researcher Award (DE130101033); Marie-Curie FP7 REA grant (PCIG-GA-2013-631543 MIRCOMB).

See Supplement 1 for supporting content.

REFERENCES

1. C. R. Petersen, U. Moller, I. Kubat, B. Zhou, S. Dupont, J. Ramsay, T. Benson, S. Sujecki, N. A. Moneim, Z. Tang, D. Furniss, A. Seddon, and O. Bang, "Mid-infrared supercontinuum covering the 1.4–13.3 μm molecular fingerprint region using ultra-high NA chalcogenide step-index fibre," Nat. Photonics **8**, 830–834 (2014).
2. Y. Yu, X. Gai, P. Ma, D.-Y. Choi, Z. Yang, R. Wang, S. Debbarma, S. J. Madden, and B. Luther-Davies, "A broadband, quasi-continuous, mid-infrared supercontinuum generated in a chalcogenide glass waveguide," Laser Photon. Rev. **8**, 792–798 (2014).
3. C. Koos, P. Vorreau, T. Vallaitis, P. Dumon, W. Bogaerts, R. Baets, B. Esembeson, I. Biaggio, T. Michinobu, F. Diederich, W. Freude, and J. Leuthold, "All-optical high-speed signal processing with silicon-organic hybrid slot waveguides," Nat. Photonics **3**, 216–219 (2009).
4. B. Jalali and S. Fathpour, "Silicon photonics," J. Lightwave Technol. **24**, 4600–4615 (2006).
5. M. J. R. Heck, H. W. Chen, A. W. Fang, B. R. Koch, D. Lang, M. N. Sysak, and J. E. Bowers, "Hybrid silicon photonics for optical interconnects," IEEE J. Sel. Top. Quantum Electron. **17**, 333–346 (2011).
6. A. B. Redondo, C. Husko, D. Eades, Y. Zhang, J. Li, T. F. Krauss, and B. J. Eggleton, "Observation of soliton compression in silicon photonic crystals," Nat. Commun. **5**, 3160 (2011).
7. Q. Lin and G. P. Agrawal, "A silicon waveguides for creating quantum-correlated photon pairs," Opt. Lett. **31**, 3140–3142 (2006).
8. J. E. Sharping, K. F. Lee, M. A. Foster, A. C. Turner, B. S. Schmidt, M. Lipson, A. L. Gaeta, and P. Kumar, "Generation of correlated photons in nanoscale silicon waveguides," Opt. Express **14**, 12388–12393 (2006).
9. X. Liu, R. M. Osgood, Jr., Y. A. Vlasov, and W. M. J. Green, "Mid-infrared optical parametric amplifier using silicon nanophotonic waveguides," Nat. Photonics **4**, 557–560 (2010).
10. S. Zlatanovic, J. S. Park, S. Moro, J. M. C. Boggio, I. B. Divliansky, N. Alic, S. Mookherjea, and S. Radic, "Mid-infrared wavelength conversion in silicon waveguides using ultracompact telecom-band-derived pump source," Nat. Photonics **4**, 561–564 (2010).
11. B. Kuyken, X. Liu, R. M. Osgood, R. Baets, G. Roelkens, and W. M. J. Green, "Mid-infrared to telecom-band supercontinuum generation in highly nonlinear silicon-on-insulator wire waveguides," Opt. Express **19**, 20172–20181 (2011).
12. R. K. W. Lau, M. R. E. Lamont, A. G. Griffith, Y. Okawachi, M. Lipson, and A. L. Gaeta, "Octave-spanning mid infrared supercontinuum generation in silicon nanowaveguides," Opt. Lett. **39**, 4518–4521 (2014).
13. B. Kuyken, T. Ideguchi, S. Holzner, M. Yan, T. W. Hansch, J. V. Campenhout, P. Verheyen, S. Coen, F. Leo, R. Baets, G. Roelkens, and N. Picque, "An octave-spanning mid-infrared frequency comb generated in a silicon nanophotonic wire waveguide," Nat. Commun. **6**, 6310 (2015).
14. A. G. Griffith, R. K. W. Lau, J. Cardenas, Y. Okawachi, A. Mohanty, R. Fain, Y. H. D. Lee, M. Yu, C. T. Phare, C. B. Poitras, A. L. Gaeta, and M. Lipson, "Silicon-chip mid-infrared frequency comb generation," Nat. Commun. **6**, 6299 (2015).
15. R. A. Soref, S. J. Emelett, and W. R. Buchwald, "Silicon waveguided components for the long-wave infrared region," J. Opt. A **8**, 840–848 (2006).
16. M. Brun, P. Labeye, G. Grand, J. M. Hartmann, F. Boulila, M. Carras, and S. Nicoletti, "Low loss SiGe graded index waveguides in mid-IR application," Opt. Express **22**, 508–518 (2014).
17. T. B. Jones, A. Spott, R. Ilic, A. Spott, B. Penkov, W. Asher, and M. Hochberg, "Silicon-on-sapphire integrated waveguides for the mid-infrared," Opt. Express **18**, 12127–12135 (2010).
18. R. J. Shankar, B. Irfan, and M. Loncar, "Integrated high-quality factor silicon-on-sapphire ring resonators for the mid-infrared," Appl. Phys. Lett. **102**, 051108 (2013).
19. A. L. Spott, Y. Liu, T. B. Jones, R. Ilic, and M. Hochberg, "Silicon waveguides and ring resonators at 5.5 μm," Appl. Phys. Lett. **97**, 213501 (2010).
20. C. Y. Wong, Z. Cheng, X. Chen, K. Ku, C. K. Y. Fung, Y. M. Chen, and H. K. Tsang, "Characterization of mid-infrared silicon-on-sapphire microring resonators with thermal tuning," IEEE Photon. J. **4**, 1095–1102 (2012).

21. Y. Zou, H. Subbaraman, S. Chakravarty, X. Xu, A. Hosseini, W. C. Lai, P. Wray, and R. T. Chen, "Grating-coupled silicon-on-sapphire integrated slot waveguides operating at mid-infrared wavelengths," Opt. Lett. **39**, 3070–3073 (2014).
22. F. Li, S. D. Jackson, C. Grillet, E. Magi, D. Hudson, S. J. Madden, Y. Moghe, C. O'Brien, A. Read, S. G. Duvall, P. Atanackovic, B. J. Eggleton, and D. J. Moss, "Low propagation loss silicon-on-sapphire waveguides for the mid-infrared," Opt. Express **19**, 15212–15220 (2011).
23. G. Imthurn, "The History of Silicon-on-Sapphire," Peregrine Semiconductor white paper, 2006.
24. X. Gai, Y. Yu, B. Kuyken, P. Ma, S. J. Madden, J. V. Campenhout, P. Verheyen, G. Roelkens, R. Baets, and B. L. Davies, "Nonlinear absorption and refraction in crystalline silicon in the mid-infrared," Laser Photon. Rev. **7**, 1054–1064 (2013).
25. T. Wang, N. Venkatram, J. Gosciniak, Y. Cui, G. Qian, W. Ji, and D. T. H. Tan, "Multi-photon absorption and third-order nonlinearity in silicon at mid-infrared wavelengths," Opt. Express **21**, 32192–32198 (2013).
26. S. Pearl, N. Rotenberg, and H. M. van Driel, "Three photon absorption in silicon for 2300-3300 nm," Appl. Phys. Lett. **93**, 131102 (2008).
27. R. Soref, "Mid-infrared photonics in silicon and germanium," Nat. Photonics **4**, 495–497 (2010).
28. L. Yin, Q. Lin, and G. P. Agrawal, "Soliton fission and supercontinuum generation in silicon waveguides," Opt. Lett. **32**, 391–393 (2007).
29. L. L. Lee, D. R. Lim, L. C. Kimerling, J. Shin, and C. Franco, "Fabrication of ultralow-loss Si/SiO_2 waveguides by roughness reduction," Opt. Lett. **26**, 1888–1890 (2001).
30. D. K. Sparacin, S. J. Spector, and L. C. Kimerling, "Silicon waveguide sidewall smoothing by wet chemical oxidation," J. Lightwave Technol. **23**, 2455–2461 (2005).
31. M. Borselli, T. J. Johnson, and O. Painter, "Measuring the role of surface chemistry in silicon microphotonics," Appl. Phys. Lett. **88**, 131114 (2006).
32. P. O. Pronko, P. A. VanRompay, C. Horvath, F. Loesel, T. Juhasz, X. Liu, and G. Mourou, "Avalanche ionization and dielectric breakdown in silicon with ultrafast laser pulses," Phys. Rev. B **58**, 2387–2390 (1998).
33. A. Vaidyanathan, T. Walker, and A. H. Guenther, "The relative roles of avalanche multiplication and multiphoton absorption in laser-induced damage of dielectrics," IEEE J. Sel. Top. Quantum Electron. **16**, 89–93 (1980).
34. S. Afshar and T. M. Monro, "A full vectorial model for pulse propagation in emerging waveguides with subwavelength structures part I: Kerr nonlinearity," Opt. Express **17**, 2298–2318 (2009).
35. J. M. Dudley, G. Genty, and S. Coen, "Supercontinuum generation in photonic crystal fiber," Rev. Mod. Phys. **78**, 1135–1184 (2006).
36. A. Major, F. Yoshino, I. Nikolakakos, J. S. Aitchison, and P. W. E. Smith, "Dispersion of the nonlinear refractive index in sapphire," Opt. Lett. **29**, 602–604 (2004).
37. A. Husakou and J. Herrmann, "Supercontinuum generation of higher-order solitons by fission in photonic crystal fibers," Phys. Rev. Lett. **87**, 203901 (2001).
38. J. Herrmann, U. Griebner, N. Zhavoronkov, A. Husakou, D. Nickel, J. C. Knight, W. J. Wadsworth, P. St. J. Russell, and G. Korn, "Experimental evidence for supercontinuum generation by fission of higher-order solitons in photonic fibers," Phys. Rev. Lett. **88**, 173901 (2002).
39. G. P. Agrawal, *Nonlinear Fiber Optics* (Academic, 2012), Chap. 12.
40. M. Pradhan, R. Garg, and M. Arora, "Multiphonon infrared absorption in silicon," Phys. Rev. Lett. **27**, 25–30 (1987).
41. J. M. Dudley and S. Coen, "Coherence properties of supercontinuum spectra generated in photonic crystal and tapered optical fibers," Opt. Lett. **27**, 1180–1182 (2002).
42. J. I. Dadap, N. C. Panoiu, X. Chen, I. W. Hsieh, X. Liu, C. Y. Chou, E. Dulkeith, S. J. McNab, F. Xia, W. M. J. Green, L. Sekaric, Y. A. Vlasov, and R. M. Osgood, "Nonlinear-optical phase modification in dispersion-engineered Si photonic wires," Opt. Express **16**, 1280–1299 (2008).
43. Z. Cheng, X. Chen, C. Y. Wong, K. Xu, and H. K. Sang, "Mid-infrared suspended membrane waveguide and ring resonator on silicon-on-insulator," IEEE Photon. Technol. Lett. **4**, 1510–1519 (2012).
44. N. Singh, D. D. Hudson, and B. J. Eggleton, "Silicon-on-sapphire pillar waveguides for Mid-IR supercontinuum generation," Opt. Express **23**, 17345–17354 (2015).
45. Y. H. Lo, R. J. Deri, J. Harbison, B. J. Skromme, M. Seto, D. M. Hwang, and T. P. Lee, "GaAs-on-InP heteroepitaxial waveguides grown by molecular beam epitaxy," Appl. Phys. Lett. **53**, 1242–1244 (1988).